Eur. Phys. J. A **13**, 281–284 (2002)

THE EUROPEAN PHYSICAL JOURNAL A

Short Note

Selective laser ionization of N $\geq$ 82 indium isotopes: The new r-process nuclide ^{135}In

I. Dillmann[1], M. Hannawald[1], U. Köster[2], V.N. Fedoseyev[2], A. Wöhr[3], B. Pfeiffer[1], D. Fedorov[4], J. Shergur[3], L. Weissman[2], W.B. Walters[3], and K.-L. Kratz[1,a]

[1] Institut für Kernchemie, Universität Mainz, D-55128 Mainz, Germany
[2] CERN, CH-1211 Geneva 23, Switzerland
[3] Department of Chemistry, University of Maryland, College Park, MD 20742, USA
[4] Petersburg Nuclear Physics Institute, RUS-188350, Gatchina, Russia

Received: 17 January 2002
Communicated by J. Äystö

Abstract. Production yields and β-decay half-lives ($T_{1/2}$) of very neutron-rich indium isotopes were determined at CERN/ISOLDE using isobaric selectivity of a resonance-ionization laser ion-source. Beta-delayed neutron (βdn) multiscaling measurements have yielded improved $T_{1/2}$ for 206(6) ms ^{132}In, 165(3) ms ^{133}In and 141(5) ms ^{134}In. With 92(10) ms ^{135}In, a new r-process nuclide has been identified which acts as an important "waiting point" in the In isotopic chain for neutron densities in the range $n_{\rm n} \simeq 10^{24}$–10^{26} n/cm^3, where the r-matter flow has already passed the $A \simeq 130$ abundance peak region.

PACS. 21.10.Tg Lifetimes – 27.60.+j $90 \leq A \leq 149$ – 25.85.Ec Neutron-induced fission – 32.80.Fb Photoionization of atoms and ions

1 Introduction

The region around the neutron-rich, double-magic isotope ^{132}Sn has been the subject of intensive experimental investigations in recent years. The reason for this interest is in principle twofold. First, the evolution of the single-particle strutures over nearly 40 mass units between nuclides with $N/Z \simeq 1.0$ and isotopes with $N/Z \geq 1.6$ provides an opportunity to develop a unique microscopic approach to nuclear structure with predictive power towards nuclei at the particle drip lines which are not currently accessible for experimental study. The second motivation is related to the rapid neutron capture (r-process) nucleosynthesis of elements beyond iron. The solar-system r-abundances ($N_{\rm r,\odot}$) in the $A \simeq 130$ peak region reflect one of the three neutron magic numbers ($N = 50$, 82 and 126), where the r-matter flow is delayed by climbing up the staircases at the shell closure from presumably ^{125}Tc ($Z = 43$) to ^{130}Cd ($Z = 48$) which act with their relatively "long" β-decay half-lives as classical waiting-point nuclei. Having reached the top of the $N_{\rm r,\odot}$ peak, the r-process is able to escape the $A \simeq 130$, $N = 82$ "bottle-neck" area in the In ($Z = 49$) isotopic chain and speeds up again towards the rare-earth region. Hence, the odd-mass, even-N indium nuclei ^{131}In, ^{133}In and ^{135}In are the most important waiting-point isotopes in the high-mass wing of the $N_{\rm r,\odot}$ peak. For recent reviews about the nuclear structure and astrophysical importance of the ^{132}Sn region, see, *e.g.* [1–3].

In this paper, we report the first results of a study of the decay of the $N \geq 82$ isotopes $^{132\text{-}135}$In obtained with considerably enhanced ionization efficiency by laser ionization at CERN/ISOLDE. Beta-delayed neutron measurements were used to determine In production yields and half-lives.

2 Production

2.1 "Converter target"

Neutron-rich medium-mass nuclei are normally produced at ISOLDE by high-energy (1 or 1.4 GeV) proton-induced fission of ^{238}U. However, with this production mechanism also neutron-deficient isobars will be formed by spallation and high-energy fission. The situation is particularly complicated in the mass regions $A \simeq 80$ and 130, where the weakly produced exotic neutron-rich nuclei of interest (*e.g.*, the isotopes around ^{78}Ni and ^{132}Sn) are covered by many orders of magnitude higher background of the

[a] e-mail: kl.kratz@uni-mainz.de

surface-ionized and therefore difficult to suppress proton-rich isobars of rubidium and caesium, respectively. Fission induced by low- to medium-energy neutrons, however, does not create this problem. Such neutrons can be produced efficiently by high-energy proton spallation of heavy target materials, *e.g.*, tantalum or tungsten. The use of a "mini-spallation neutron source" (called "converter") surrounded by a concentric ISOL fission target was first proposed by Nolen *et al.* [4]. While the realization of a concentric target requires sophisticated engineering, it is relatively easy to build a reduced version by just installing a heavy-metal rod close to a standard ISOLDE fission target. In this experiment, a 10 mm diameter tantalum rod of 150 mm length was mounted parallel to the ^{238}U target at a distance of 21 mm axis-to-axis [5]. Only part of the neutrons produced in the converter will impinge on the ISOL target, but the primary beam and most of the high-energy secondary particles are located in a forward cone not hitting the target.

For this experiment a standard ISOLDE UC_x/graphite target [6] with 50 g/cm^2 ^{238}U and about 10 g/cm^2 carbon was used. The target was kept at 2150 °C and the niobium ionizer line at 1850 °C. Pulses of 1.4 GeV protons (5.3 μC each) were hitting the tantalum converter every 2.4 s.

2.2 Ionization

Indium (with an ionization potential of 5.79 eV) is already surface ionized. But, to further enhance the ionization efficiency, the ISOLDE Resonance Ionization Laser Ion Source (RILIS) [7–9] was tuned to excite In in two steps: with a frequency-doubled dye-laser beam of 303.9 nm from the $^2P^0_{1/2}$ atomic ground state to the $^2D^0_{3/2}$ excited state, and then with the green and yellow copper vapor laser beams (510.6 nm and 578.2 nm) non-resonantly to the continuum. This RILIS excitation scheme had been developed at Troitsk [10] and was already used at ISOLDE to ionize the neutron-deficient isotopes $^{100\text{-}114}$In [11].

The laser beams were focussed into the ion-source cavity, which consisted of a niobium tube of 30 mm length and 3 mm internal diameter. The average powers of the laser beams delivered to the ion source were 50 mW and 4 W, respectively, for the first and second step. The linewidth of the dye-laser radiation was rather broad, about 10 GHz, allowing the operation of RILIS with the same laser wavelengths for different isotopes without any correction for the hyperfine structure or the isotopic shifts.

With this setup, the use of the RILIS allowed to increase the In yields by about a factor seven compared to pure surface ionization. The absolute ionization efficiency could not be determined in this experiment, but it is expected to be several percent. Since the target was not equipped with a stable indium "mass marker", the RILIS had to be tuned "blindly", therefore not necessarily guaranteeing optimum efficiency. Under standard operation conditions (more copper vapor laser power focussed to the ionizer, and simultaneous excitation of the thermally populated $^2P^0_{3/2}$ state with a second dye-laser [11]), the ionization efficiency could probably be further enhanced by at least another factor three.

Table 1. Yields of heavy indium isotopes from a 50 g/cm^2 UC_x/graphite target with the RILIS tuned for indium ionization. The yield Y is given in ions per μC of primary proton beam [13] hitting the tantalum "converter" rod.

Isotope	^{130}In	^{132}In	^{133}In	^{134}In	^{135}In
Y (μC^{-1})	$> 3.5 \cdot 10^5$	8000	900	≈ 95	≈ 2.4

2.3 Yields

Table 1 shows the observed yields of the most neutron-rich indium isotopes deduced from the measured β- (^{130,132}In) and βdn activities ($^{133\text{-}135}$In), respectively. For ^{133}In the branching ratio for βdn emission ($P_n = 85\%$) was taken from [12] and for ^{134,135}In we used the theoretical P_n values of 93% and 95%, respectively, obtained from our QRPA calculations (see below). All quoted yields were integrated over the complete release curve and are normalized to 1 μC of primary protons as defined in [13].

3 Results and discussion

3.1 Half-lives

After laser ionization and mass separation, the isotopically clean beams of In nuclides were transported to a beam line equipped with a moving tape system where βdn measurements could be performed. Counting took place directly at the point of deposit, and the tape system was used to remove the activities of the longer-lived daughter nuclides. Because the In half-lives being sought are in the 100 ms range, data acquisition in the system was initiated by the CERN-PSB proton pulses, separated by a multiple of 2.4 s, and continued for 1.6 s for each cycle.

Beta-delayed neutron data were collected by multiscaling measurements using the high-efficiency Mainz 4π ^{3}He neutron long-counter. This detector was equipped with 64 ^{3}He proportional counters arranged in three concentric rings. The βdn multiscaling data were analyzed with a multicomponent least-squares fit to obtain the In half-lives by taking into account the known βdn contributions from the Sn daughter products at masses A and $(A-1)$ [14–16] and a small constant neutron background. The resulting net βdn-decay curves for $^{133\text{-}135}$In are shown in fig. 1. The $T_{1/2}$ values are summarized in table 2, and are compared to literature values and predictions from two Quasi-Particle Random-Phase Approximation (QRPA) models. The first one is in principle a "deformed" QRPA [17] for Gamow-Teller (GT) decay, which takes the ground-state shape of the β-decay daughter isotopes as predicted by the Finite-Range Droplet Model (FRDM) [18]. This QRPA version uses experimental nuclear masses as far as they are available [14] and otherwise FRDM predictions. The second GT strength-function model is the so-called continuum QRPA (cQRPA) of Borzov *et al.* (see, *e.g.* [19])

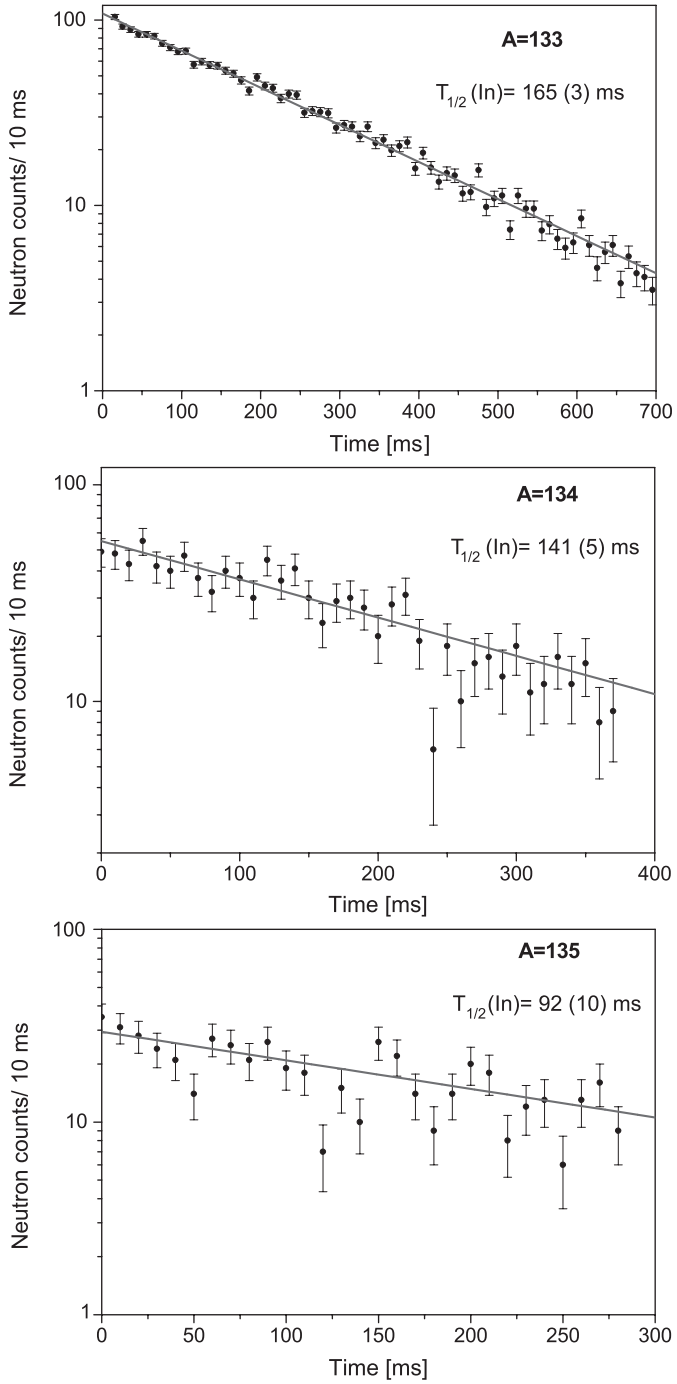

Fig. 1. Beta-delayed neutron decay curves for the neutron-rich isotopes $^{133\text{-}135}$In, after correction for βdn-daughter activities and neutron background.

which is limited to spherical nuclei. It uses nuclear mass predictions from the ETFSI model [20].

The comparison of the experimental In half-lives listed in table 2 with the predictions derived from the QRPA calculations of GT strength functions [18,19] indicates a satisfactory agreement within about a factor two. The differences between the QRPA and cQRPA predictions mainly reflect the effects from the different pairing models used

Table 2. Comparison of experimental β-decay half-lives ($T_{1/2}$) for $^{132\text{-}135}$In with literature values and QRPA predictions for Gamow-Teller (GT) decay [18,19]. For further discussion, see text.

Mass	Half-life (ms)				
	This work	Literature	Ref.	QRPA	cQRPA
132	206(6)	201(13)	[15]	96	212
133	165(3)	180(20)	[15]	141	245
134	141(5)	138(8)	[21]	99	190
135	92(10)	–	–	90	251

(Lipkin-Nogami in [17], and BCS in [20]) and the different Q_β values. To give an example, for ^{132}In Audi *et al.* [14] give an experimental Q_β value of 14.13 MeV, which is roughly 1 MeV higher than the predictions of both mass models, FRDM [18] and ETFSI [20]. Using this experimental Q_β value, our QRPA calculates a $T_{1/2}(\mathrm{GT}) = 96$ ms, as listed in table 2. When using the theoretical Q_β values from FRDM or ETFSI instead, with our QRPA model we would obtain about a factor two longer $T_{1/2}$(GT) of 181 ms and 164 ms, respectively. Actually, it is this latter half-life from the lower Q_β value of ETFSI (13.23 MeV) that should be compared to the cQRPA prediction of 212 ms, which is in better agreement with the experimental $T_{1/2} = 206$ ms. This example shows, however, that "better agreement with experiment" may turn out to be fortuitous and does not necessarily mean that the underlying theoretical model is better.

3.2 r-process abundances

With respect to rapid neutron capture nucleosynthesis (the r-process), among nuclear data β-decay properties ($T_{1/2}$ and P_n values) and masses (in particular neutron separation energies, S_n values) are the most important input parameters for astrophysical calculations [22,23]. As is shown in fig. 2, the isotopes $^{131}\mathrm{In}_{82}$, $^{133}\mathrm{In}_{84}$, $^{135}\mathrm{In}_{86}$, etc. are the major waiting-point nuclides in the region just beyond the $A \simeq 130$ $N_{\mathrm{r},\odot}$ peak, carrying the main progenitor abundances prior to β-decay. It is furthermore seen from this figure that the odd-neutron In isotopes (with "low" S_n values) only build up small progenitor abundances. The reason for this is that as soon as they have been formed in rapid neutron capture, the odd-neutron isotopes will not have time to β-decay but either capture an additional neutron to become an $(A+1)$ even-neutron nuclide or photodisintegrate back to an $(A-1)$ even-neutron In isotope (both with "high" S_n values) for which now β-decay is the fastest reaction. As a consequence, the $T_{1/2}$ of these even-neutron isotopes are of major importance in the waiting-point concept, which implies the historical $N_{\mathrm{r},\odot}(Z) \times \lambda(Z) \simeq$ const correlation.

In fig. 2, we show the absolute r-abundances (normalized to $Si = 10^6$) of the $82 \leq N \leq 90$ In progenitors obtained from our standard multicomponent, time-dependent calculations (see, *e.g.* [24,1]) for a freeze-out temperature of $T_9 = 1.35$ and assuming Fe as the seed element.

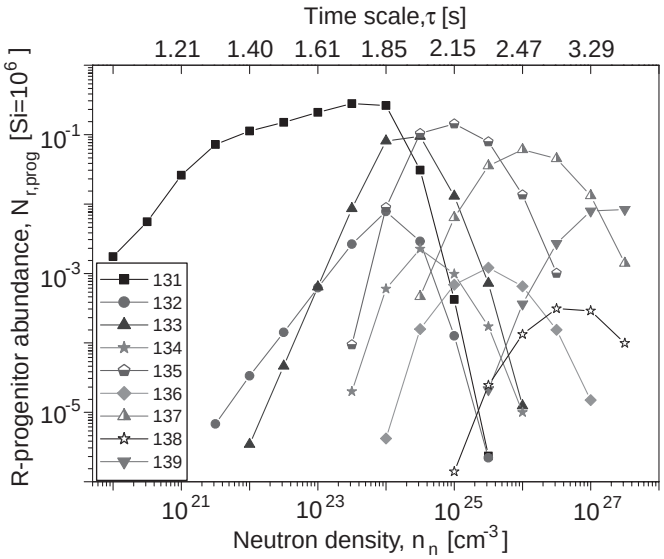

Fig. 2. r-process progenitor abundances of $N \geq 82$ indium isotopes at freeze-out conditions ($T_9 = 1.35$) as a function of neutron density. For details, see text.

Depending on the neutron density ($n_{\rm n}$) and the corresponding process duration (τ), different even-neutron In isotopes act as main waiting points. For modest neutron densities of $n_{\rm n} \simeq 10^{20}$–10^{24} n/cm^3, representative for overpassing the $A \simeq 80$ $N_{\rm r\odot}$ peak and forming the second peak at $A \simeq 130$, neutron-magic ^{131}In is the waiting point. At about $n_{\rm n} = 10^{24}$ n/cm^3 and a process duration of 2.15 s, all major $N = 82$ r-progenitors below ^{132}Sn, from ^{126}Ru to ^{131}In have reached their approximate maximum abundances, thus reflecting the "bottle-neck" behavior of the neutron shell closure for the r-matter flow. When using an $A \simeq 90$ seed composition, as suggested by the neutrino wind SN II scenario [24], the r-process avoids the delay of the matter flow by the $N = 50$ waiting-point isotopes ^{78}Ni to ^{81}Ga, and the above flow time reduces to about 350 ms. Our new $N = 86$ isotope ^{135}In becomes the main waiting point in the In chain at neutron densities around $n_{\rm n} \simeq 10^{25}$ n/cm^3, where the r-process has already succeeded to break through the $N = 82$ shell. Because of the expected high $P_{\rm n}$ value of ^{135}In, after freeze-out and β-decay back to stability, most of the $A = 135$ progenitor abundance will show up at $(A-1)$, *i.e.* as ^{134}Xe in the solar r-abundance curve. As is also seen from fig. 2, for $n_{\rm n} \geq 3 \times 10^{25}$ n/cm^3, the even-N isotopes ^{137}In and ^{139}In take over as waiting points, however with decreasing abundances. Again, because of their predicted high $P_{\rm n}$ values they will be the main progenitors of the $(A-1)$ stable r-isotopes ^{136}Xe and ^{138}Ba, respectively.

4 Summary

In this paper, we have presented production yields and β-decay half-lives of very neutron-rich In isotopes, including the new r-process waiting-point nucleus ^{135}In. These data, together with our recent results on neutron-rich Ag, Cd and Sn isotopes around doubly magic ^{132}Sn (see, *e.g.* [1,3,16,25–27]) have considerably improved our nuclear-structure knowledge in this interesting region. However, more detailed spectroscopic information is still needed; and in fact such experiments are underway by our collaboration at CERN/ISOLDE. The study of the β-decay properties of the main $N \simeq 82$ r-process waiting-point isotopes has undoubtedly led to a better understanding of the astrophysical conditions for the formation of the $A \simeq 130$ $N_{\rm r,\odot}$ peak [28]. Nevertheless, measurements of nuclear masses are still needed below and beyond ^{132}Sn in order to obtain a completely experimental nuclear-data input in this important "bottle-neck" region of the r-process matter flow.

We would like to thank the German BMBF (06MZ9631), the EU TMR (ERBFMGECT 980120) and the U.S. Department of Energy for financial support of our experiments, and the GSI for partial funding of our astrophysics calculations.

References

1. K.-L. Kratz *et al.*, Hyperfine Interact. **129**, 185 (2000).
2. H. Mach, Acta Phys. Pol. B **32**, 887 (2001).
3. B. Pfeiffer *et al.*, Nucl. Phys. A **693**, 282 (2001).
4. J.A. Nolen *et al.*, AIP Conf. Proc. Vol. **473** (AIP, New York, 1998) p. 477.
5. R. Catherall *et al.*, in *Proceedings ENAM'01* (Springer Verlag) in press.
6. H.L. Ravn *et al.*, Nucl. Instrum. Methods B **26**, 183 (1987).
7. V.I. Mishin *et al.*, Nucl. Instrum. Methods **B73**, 550 (1993).
8. V.N. Fedoseyev *et al.*, Hyperfine Interact. **127**, 409 (2000).
9. U. Köster, in *Proceedings RNB-5*, to be published in Nucl. Phys. A **701**, (2002).
10. M.L. Muchnik *et al.*, Sov. J. Quantum Electron. **13**, 1515 (1983).
11. U. Köster, in *Proceedings ENAM'01*, to be published in Eur. Phys. J. A (2002).
12. B. Pfeiffer *et al.*, to be published in Prog. Nucl. Energy (2002); `http://www.arXiV.org/abs/nucl-ex/0106020`.
13. J. Lettry *et al.*, Nucl. Instrum. Methods B **126**, 130 (1997).
14. G. Audi *et al.*, Nucl. Phys. A **634**, 1 (1997).
15. R.B. Firestone *et al.*, *Table of Isotopes*, 8th edition (Wiley, New York, 1996).
16. J. Shergur *et al.*, Nucl. Phys. A **682**, 493 (2001); Phys. Rev. C **65**, 034312 (2002).
17. P. Möller, J. Randrup, Nucl. Phys. A **514**, 1 (1990).
18. P. Möller *et al.*, At. Data Nucl. Data Tables **59**, 183 (1995); **66**, 131 (1997).
19. I. Borzov, S. Goriely, Phys. Rev. C **62**, 035501 (2000).
20. Y. Aboussir *et al.*, At. Data Nucl. Data Tables **61**, 127 (1995).
21. P. Hoff *et al.*, Phys. Rev. Lett. **77**, 1020 (1996).
22. E.M. Burbidge *et al.*, Rev. Mod. Phys. **29**, 547 (1957).
23. K.-L. Kratz *et al.*, Astrophys. J. **403**, 216 (1993).
24. C. Freiburghaus *et al.*, Astrophys. J. **516**, 381 (1999).
25. M. Hannawald *et al.*, Phys. Rev. C **62**, 054301 (2000).
26. T. Kautzsch *et al.*, Phys. Rev. C **54**, 2811 (1996).
27. T. Kautzsch *et al.*, Eur. Phys. J. A **9**, 201 (2000).
28. K.-L. Kratz, Nucl. Phys. A **688**, 308c (2001).